



This is the accepted manuscript made available via CHORUS. The article has been published as:

Magnetic structure of few-nucleon systems at high momentum transfers in a chiral effective field theory approach

A. Gnech and R. Schiavilla

Phys. Rev. C **106**, 044001 — Published 7 October 2022

DOI: 10.1103/PhysRevC.106.044001

Magnetic structure of few-nucleon systems at high momentum transfers in a χEFT approach

A. Gnech^a and R. Schiavilla^{a,b},

^a Theory Center, Jefferson Lab, Newport News, Virginia 23606, USA

^b Department of Physics, Old Dominion University, Norfolk, Virginia 23529, USA

(Dated: September 13, 2022)

The five low-energy constants (LECs) in the electromagnetic current derived in chiral effective field theory (χ EFT) up to one loop are determined by a simultaneous fit to the A=2-3 nuclei magnetic moments and to the deuteron magnetic form factor and threshold electrodisintegration at backward angles over a wide range of momentum transfers. The resulting parametrization then yields predictions for the 3 He/ 3 H magnetic form factors in excellent accord with the experimental values for momentum transfers ranging up to ≈ 0.8 GeV/c, beyond the expected regime of validity of the χ EFT approach. The calculations are based on last-generation two-nucleon interactions including high orders in the chiral expansion and derived by Entem, Machleidt, and Nosyk [Phys. Rev. C 96, 024004 (2017)] and by Piarulli et al. [Phys. Rev. C 94, 054007 (2016)], using different χ EFT formulations. In the A=3 calculations, (chiral) three-nucleon interactions are also accounted for. The model dependence resulting from these different formulations of the interactions is found to be mild for momentum transfer below ≈ 0.8 GeV/c. An analysis of the convergence of the chiral expansion is also provided.

I. INTRODUCTION AND CONCLUSIONS

The nuclear electromagnetic current derived in chiral effective field theory (χEFT) at one loop is characterized by five low-energy constants (LECs). Three of these LECs enter a subleading one-pion-exchange (OPE) term, while the remaining two are associated with contact terms induced by non-minimal coupling to the electromagnetic field. Resonance saturation arguments can be used [4] (and have been used [8, 15]) to relate the two LECs in the isovector component of the subleading OPE current to the N-to- Δ transition axial coupling and transition magnetic moment. The remaining LECs have been determined by fitting experimentally known few-nucleon observables at low energy and momentum transfers, such as the magnetic moments of deuteron, ³H, and ³He [8, 15] and/or the deuteron magnetic form factor [1] and/or the cross section for radiative capture of thermal neutrons on protons [8].

In the present work we adopt a different strategy for constraining these LECs: (i) we do not invoke resonance saturation, and (ii) we determine the complete set of five LECs by a simultaneous fit to the magnetic moments of the A = 2-3 nuclei, and the deuteron magnetic form factor and threshold electrodisintegration cross section at backward angles over a wide range of momentum transfers. It turns out that these five LECs provide enough flexibility to allow us to reproduce well all these observables in a region of momentum transfers that extends above 4 fm⁻¹. That a satisfactory fit of these high momentum transfer data is possible, was not anticipated. It suggests that the present parametrization of the current is robust in kinematical regimes (momentum transfers of the order of 0.8 GeV/c) outside the limits of validity of the χ EFT expansion. This conclusion is further corroborated by the excellent agreement between the measured and predicted magnetic form factors of $^3\mathrm{H}/^3\mathrm{He}$ for momentum transfers up to 0.8 GeV/c, including partially their diffraction regions. Previous parametrizations of the $\chi\mathrm{EFT}$ current, using resonance saturation arguments and based on fits of static magnetic properties of deuteron and trinucleons, had failed to provide a good description of these regions [8, 15].

The present paper is organized as follows. In the next section we list the expressions for the $\chi \rm EFT$ current up to one loop. These are well known by now, but are reported here for completeness and to facilitate the ensuing discussions. In Sec. III we detail the determination of the LECs and associated uncertainties, and in Sec. IV we present a comparison between the measured trinucleon magnetic form factors and those predicted by the present parametrization of the $\chi \rm EFT$ current. We also show in that section that the (crucial) two-body terms in the current yield contributions in the deuteron threshold electrodisintegration and A=3 magnetic form factors that are proportional to each other. The implications of this fact are discussed.

II. EM CURRENTS UP TO ONE LOOP

Independent derivations of nuclear electromagnetic current and charge operators up to one loop in χEFT have been carried out within a variety of different formalisms and in a number of papers [2–8] in the past three decades or so. For clarity of presentation and for later reference, we report below the explicit expressions for the electromagnetic current operators of interest in the present work. We adopt the notation of Refs. [4, 8]; in particular, we denote the generic low-momentum scale with Q and the momentum due to the external electro-

magnetic field with q, and define

$$\mathbf{k}_{i} = \mathbf{p}'_{i} - \mathbf{p}_{i}$$
, $\mathbf{K}_{i} = (\mathbf{p}'_{i} + \mathbf{p}_{i})/2$, (2.1)

$$\mathbf{k} = (\mathbf{k}_1 - \mathbf{k}_2)/2$$
, $\mathbf{K} = \mathbf{K}_1 + \mathbf{K}_2$, (2.2)

where \mathbf{p}_i (\mathbf{p}_i') is the initial (final) momentum of nucleon i. We further note that in the $\mathbf{j}^{(n)}$ expressions reported below the superscript n specifies the order $e\ Q^n$ in the power counting (in a two-nucleon system). The lowest-order (LO) contribution $\mathbf{j}^{(-2)}$ consists of the single-nucleon current

$$\mathbf{j}_{\mathrm{NR}}^{(-2)}(\mathbf{q}) = \frac{e}{2 m_N} \left[2 e_{N,1}(q_\mu^2) \,\mathbf{K}_1 + i \,\mu_{N,1}(q_\mu^2) \,\boldsymbol{\sigma}_1 \times \mathbf{q} \right] \times \delta(\mathbf{p}_2' - \mathbf{p}_2) + 1 \rightleftharpoons 2 , \qquad (2.3)$$

where m_N is the nucleon mass, $\mathbf{q} = \mathbf{k}_i$ with i = 1 or 2 (the δ -function enforcing overall momentum conservation $\mathbf{q} = \mathbf{k}_1$ has been dropped for brevity here and in the following),

$$e_{N,i}(q_{\mu}^2) = \left[G_E^S(q_{\mu}^2) + G_E^V(q_{\mu}^2) \, \tau_{i,z} \right] / 2 ,$$

$$\mu_{N,i}(q_{\mu}^2) = \left[G_M^S(q_{\mu}^2) + G_M^V(q_{\mu}^2) \, \tau_{i,z} \right] / 2 , \qquad (2.4)$$

and $G_E^{S/V}$ and $G_M^{S/V}$ denote the isoscalar/isovector combinations of the proton (p) and neutron (n) electric (E) and magnetic (M) form factors

$$G_{E/M}^{S/V}(q_{\mu}^2) = G_{E/M}^p(q_{\mu}^2) + / - G_{E/M}^n(q_{\mu}^2) \; . \eqno(2.5)$$

The power counting eQ^{-2} of this current results from the product of a factor eQ due to the coupling of the external electromagnetic field to the individual nucleons, and the factor Q^{-3} from the momentum δ -function entering this type of disconnected contributions. Of course, such a counting ignores the fact that the nucleon form factors themselves also have a power series expansion in Q. Here, they are taken from fits to elastic electron scattering data off the proton and deuteron rather than derived consistently in chiral perturbation theory (χPT) [9]; specifically, we utilize the dipole parametrization with

$$\begin{split} G_E^p(q_\mu^2) \!=\! G_D(q_\mu^2) \;, \quad & G_E^n(q_\mu^2) \!=\! -\mu^n \, \frac{q_\mu^2}{4 \, m_N^2} \frac{G_D(q_\mu^2)}{1 + q_\mu^2/m_N^2} \;, \\ G_M^p(q_\mu^2) &= \mu^p G_D(q_\mu^2) \;, \quad & G_M^n(q_\mu^2) = \mu^n G_D(q_\mu^2) \;, \end{split}$$

where μ^p and μ^n are, respectively, the proton and neutron magnetic moments, and

$$G_D(q_\mu^2) = (1 + q_\mu^2/\Lambda^2)^{-2} ,$$
 (2.6)

with $\Lambda=0.83$ GeV. We take these form factors as functions of the four-momentum transfer $q_{\mu}^2=q^2-\omega^2$, where ω is the energy transfer. We also note that the calculation presented below are carried out in the laboratory frame.

At order n = -1 (NLO) there is a one-pion exchange (OPE) contribution that reads

$$\mathbf{j}_{\pi}^{(-1)}(\mathbf{q}) = -i \, e \frac{g_A^2}{4f_{\pi}^2} \, G_E^V(q_{\mu}^2) \, (\boldsymbol{\tau}_1 \times \boldsymbol{\tau}_2)_z \bigg(\boldsymbol{\sigma}_1 - \mathbf{k}_1 \, \frac{\boldsymbol{\sigma}_1 \cdot \mathbf{k}_1}{\omega_{k_1}^2} \bigg)$$

$$\times \frac{\sigma_2 \cdot \mathbf{k}_2}{\omega_{k_2}^2} + 1 \rightleftharpoons 2 , \qquad (2.7)$$

where g_A is the nucleon axial coupling constant $(g_A=1.29),\ f_\pi$ is the pion decay amplitude $(f_\pi=92.4\ \mathrm{MeV})$ and we have defined $\omega_k^2=k^2+m_\pi^2$, with m_π being the pion mass. The inclusion of the isovector electric form factor $G_E^V(q_\mu^2)$ in $\mathbf{j}^{(-1)}$ can be justified on the basis of the continuity equation, see Ref. [8].

Relativistic corrections to the leading order one-body current operators enter at n = 0 (denoted as N2LO), and are given by

$$\mathbf{j}_{\mathrm{RC}}^{(0)}(\mathbf{q}) = -\frac{e}{8 \, m_N^3} e_{N,1}(q_\mu^2) \left[2 \left(K_1^2 + q^2/4 \right) \left(2 \, \mathbf{K}_1 + i \, \boldsymbol{\sigma}_1 \times \mathbf{q} \right) + \mathbf{K}_1 \cdot \mathbf{q} \left(\mathbf{q} + 2 \, i \, \boldsymbol{\sigma}_1 \times \mathbf{K}_1 \right) \right]$$

$$-\frac{i \, e}{8 \, m_N^3} \left[\mu_{N,1}(q_\mu^2) - e_{N,1}(q_\mu^2) \right] \left[\mathbf{K}_1 \cdot \mathbf{q} \qquad (2.8) \right]$$

$$\times \left(4 \, \boldsymbol{\sigma}_1 \times \mathbf{K}_1 - i \, \mathbf{q} \right) - \left(2 \, i \, \mathbf{K}_1 - \boldsymbol{\sigma}_1 \times \mathbf{q} \right) \, q^2/2$$

$$+2 \left(\mathbf{K}_1 \times \mathbf{q} \right) \, \boldsymbol{\sigma}_1 \cdot \mathbf{K}_1 \left[\delta(\mathbf{p}_2' - \mathbf{p}_2) + 1 \rightleftharpoons 2 \right].$$

In the calculations of electromagnetic observables to follow, we also utilize chiral 2N and 3N interactions which retain explicitly Δ -isobar degrees of freedom, the NV models of Refs. [10–12]. In these instances, we account for the N2LO currents originating from explicit Δ intermediate states, given by [3]

$$\mathbf{j}_{\Delta}^{(0)}(\mathbf{q}) = i e \frac{g_A h_A}{18 m_{\Delta N} f_{\pi}^2} G_{\gamma N \Delta}(q_{\mu}^2) \frac{\boldsymbol{\sigma}_2 \cdot \mathbf{k}_2}{\omega_{k_2}^2} \left[4 \tau_{2,z} \, \mathbf{k}_2 - (\boldsymbol{\tau}_1 \times \boldsymbol{\tau}_2)_z \, \boldsymbol{\sigma}_1 \times \mathbf{k}_2 \right] \times \mathbf{q} + 1 \rightleftharpoons 2 , \quad (2.9)$$

where $m_{\Delta N}$ is the Δ -nucleon mass difference ($m_{\Delta N}=293$ MeV), h_A and $G_{\gamma N\Delta}$ are, respectively, the N-to- Δ transition axial coupling constant ($h_A=2.74$) and transition electromagnetic form factor. The latter is parametrized as

$$G_{\gamma N \Delta}(q_{\mu}^2) = \frac{\mu_{\gamma N \Delta}}{(1 + q_{\mu}^2 / \Lambda_{\Delta, 1}^2)^2 \sqrt{1 + q_{\mu}^2 / \Lambda_{\Delta, 2}^2}}, \quad (2.10)$$

where $\mu_{\gamma N\Delta}$ —the transition magnetic moment—is taken to be $3 \mu_N$ from an analysis of γN data in the Δ -resonance region [13]. This analysis also gives $\Lambda_{\Delta,1}$ =0.84 GeV and $\Lambda_{\Delta,2}$ =1.2 GeV.

The currents at order $e\,Q$ (N3LO) consist of: (i) terms generated by minimal substitution in the four-nucleon contact interactions involving two gradients of the nucleon fields as well as by non-minimal couplings to the electromagnetic field; (ii) OPE terms induced by $\gamma\pi N$ interactions of sub-leading order; and (iii) one-loop two-pion-exchange (TPE) terms. We discuss them below.

The contact minimal and non-minimal currents, denoted by the subscripts "min" and "nm" respectively, are written as [8]

$$\mathbf{j}_{\min}^{(1)}(\mathbf{q}) = rac{i\,e}{16}\,G_E^V(q_\mu^2)\,\left(m{ au}_1 imesm{ au}_2
ight)_z\,\left[\left(C_2+3\,C_4+C_7
ight)\mathbf{k}_1
ight]$$

$$+(C_{2} - C_{4} - C_{7}) \mathbf{k}_{1} \boldsymbol{\sigma}_{1} \cdot \boldsymbol{\sigma}_{2}$$

$$+C_{7} \boldsymbol{\sigma}_{1} \cdot (\mathbf{k}_{1} - \mathbf{k}_{2}) \boldsymbol{\sigma}_{2} - \frac{i e}{4} e_{N,1}(q_{\mu}^{2}) C_{5}$$

$$\times (\boldsymbol{\sigma}_{1} + \boldsymbol{\sigma}_{2}) \times \mathbf{k}_{1} + 1 \rightleftharpoons 2 , \qquad (2.11)$$

$$\mathbf{j}_{nm}^{(1)}(\mathbf{q}) = -i e \left[G_{E}^{S}(q_{\mu}^{2}) C_{15}^{\prime} \boldsymbol{\sigma}_{1} + G_{E}^{V}(q_{\mu}^{2}) C_{16}^{\prime} \right]$$

$$\times (\tau_{1,z} - \tau_{2,z}) \boldsymbol{\sigma}_{1} \times \mathbf{q} + 1 \rightleftharpoons 2 . \qquad (2.12)$$

The low-energy constants (LECs) C_1, \ldots, C_7 enter the two-nucleon (2N) contact interaction (at NLO), and are constrained by fits to the np and pp elastic scattering data and the deuteron binding energy. We take their values from the various 2N interactions we have adopted in the present study (see Sec. III). We should point out that in the case of the NV models, the original parametrization of the contact interaction at NLO is subjected to a Fierz rearrangement, so as to make it local [10]. As a consequence, the LECs C_2 , C_4 , C_5 , and C_7 in Eq. (2.11) are related to those introduced in Ref. [10, 11] and denoted with a P superscript here for clarity via

$$C_2 = -4 C_2^P - 12 C_4^P + 6 C_6^P$$

$$C_4 = -4 C_2^P + 4 C_4^P + 14 C_6^P ,$$
(2.13)

 $C_5 = C_7^P$, and $C_7 = -24 \, C_6^P$. In Ref. [15] this correspondence between the C_i and C_i^P has been inadvertently ignored. The error affects the contribution labeled N3LO(MIN) in Tables III and IV, and the fitted values d_1^S , d_2^S , and d_1^V in Table I of Ref. [15]. However, we have verified that it does not significantly change the predicted values for the various observables considered in that work, or alter the ensuing discussions.

The LECs C_{15}' and C_{16}' (as well as d_8' , d_9' , and d_{21}' below) are determined by fitting measured photo-nuclear observables of the A=2 and 3 systems, as discussed in Sec. III. Finally, there is no a priori justification for the use of G_E^S/G_E^V (or G_M^S/G_M^V) in the non-minimal contact current; they are included so as to provide a reasonable fall-off with increasing q_μ^2 for the strength of this current.

The sub-leading OPE currents at N3LO have isovector (IV) and isoscalar (IS) components given by, respectively,

$$\mathbf{j}_{\pi \text{IV}}^{(1)}(\mathbf{q}) = i e \frac{g_A}{4 f_\pi^2} \frac{G_{\gamma N \Delta}(q_\mu^2)}{\mu_{\gamma N \Delta}} \frac{\boldsymbol{\sigma}_2 \cdot \mathbf{k}_2}{\omega_{k_2}^2} \left[d_8' \, \tau_{2,z} \, \mathbf{k}_2 \, (2.15) \right]$$
$$-d_{21}' \left(\boldsymbol{\tau}_1 \times \boldsymbol{\tau}_2 \right)_z \, \boldsymbol{\sigma}_1 \times \mathbf{k}_2 \times \mathbf{q} + 1 \rightleftharpoons 2 ,$$

and

$$\mathbf{j}_{\pi \text{IS}}^{(1)}(\mathbf{q}) = i \, e \, \frac{g_A}{4 \, f_\pi^2} \, d_9' \, G_{\gamma \pi \rho}(q_\mu^2) \, \boldsymbol{\tau}_1 \cdot \boldsymbol{\tau}_2 \, \frac{\boldsymbol{\sigma}_2 \cdot \mathbf{k}_2}{\omega_{k_2}^2} \, \mathbf{k}_2 \times \mathbf{q} + 1 \rightleftharpoons 2 \,,$$
(2.16)

and depend on the three (unknown) LECs d_8' , d_9' , and d_{21}' . The LECs d_8' and d_{21}' can be related [4] to the N- Δ

transition axial coupling constant and magnetic moment in a resonance saturation picture, which justifies the use of the $\gamma N\Delta$ electromagnetic form factor for this term. However, we emphasize that, in contrast to Ref. [15], Δ saturation for these LECs is not assumed here. The LEC d_9' reduces, in a resonance saturation picture, to the well known $\gamma\pi\rho$ current [4]. Accordingly, we have accounted for the q_μ^2 fall-off of the electromagnetic vertex by including a $\gamma\pi\rho$ form factor, which in vector-meson dominance is parametrized as

$$G_{\gamma\pi\rho}(q_{\mu}^2) = \frac{1}{1 + q_{\mu}^2/m_{\nu\nu}^2} ,$$
 (2.17)

where m_{ω} is the ω -meson mass.

The one-loop TPE currents are written as [4, 8]

$$\mathbf{j}_{2\pi}^{(1)}(\mathbf{q}) = -i e G_E^V(q_\mu^2) \left[(\boldsymbol{\tau}_1 \times \boldsymbol{\tau}_2)_z \, \boldsymbol{\nabla}_k \, F_1(k) - \tau_{2,z} \right]$$

$$\times \left[F_0(k) \, \boldsymbol{\sigma}_1 - F_2(k) \, \frac{\mathbf{k} \, \boldsymbol{\sigma}_1 \cdot \mathbf{k}}{k^2} \right] \times \mathbf{q} + 1 \rightleftharpoons 2 ,$$
(2.18)

where **k** is the relative momentum defined above, and the functions $F_i(k)$ are

$$F_{0}(k) = \frac{g_{A}^{2}}{128 \pi^{2} f_{\pi}^{4}} \left[1 - 2 g_{A}^{2} + \frac{8 g_{A}^{2} m_{\pi}^{2}}{k^{2} + 4 m_{\pi}^{2}} + G(k) \left[2 - 2 g_{A}^{2} - \frac{4 (1 + g_{A}^{2}) m_{\pi}^{2}}{k^{2} + 4 m_{\pi}^{2}} + \frac{16 g_{A}^{2} m_{\pi}^{4}}{(k^{2} + 4 m_{\pi}^{2})^{2}} \right] \right], \qquad (2.19)$$

$$F_{1}(k) = \frac{1}{1536 \pi^{2} f_{\pi}^{4}} G(k) \left[4 m_{\pi}^{2} (1 + 4 g_{A}^{2} - 5 g_{A}^{4}) + k^{2} (1 + 10 g_{A}^{2} - 23 g_{A}^{4}) - \frac{48 g_{A}^{4} m_{\pi}^{4}}{4 m_{\pi}^{2} + k^{2}} \right], \qquad (2.20)$$

$$F_{2}(k) = \frac{g_{A}^{2}}{128 \pi^{2} f_{\pi}^{4}} \left[2 - 6 g_{A}^{2} + \frac{8 g_{A}^{2} m_{\pi}^{2}}{k^{2} + 4 m_{\pi}^{2}} + G(k) \left[4 g_{A}^{2} - \frac{4 (1 + 3 g_{A}^{2}) m_{\pi}^{2}}{k^{2} + 4 m_{\pi}^{2}} + \frac{16 g_{A}^{2} m_{\pi}^{4}}{(k^{2} + 4 m_{\pi}^{2})^{2}} \right] \right], \qquad (2.21)$$

with the loop function G(k) defined as

$$G(k) = \frac{\sqrt{4 m_{\pi}^2 + k^2}}{k} \ln \frac{\sqrt{4 m_{\pi}^2 + k^2} + k}{\sqrt{4 m_{\pi}^2 + k^2} - k} .$$
 (2.22)

As noted in Refs. [4, 8], the expression above follows from expanding the TPE current in powers of the external field momentum ${\bf q}$ and in retaining up to linear terms in ${\bf q}$. It satisfies current conservation with the TPE 2N interaction at NLO.

 $^{^1}$ Tables of the corrected values of the $d_1^S,\,d_2^S,$ and d_1^V LECs are available upon request.

² In other words, in the present study, when using the NV interactions, we include both $\mathbf{j}_{\Delta}^{(0)}$ and $\mathbf{j}_{\pi \mathrm{IV}}^{(1)}$, whereas in Ref. [15] we only included $\mathbf{j}_{\Delta}^{(0)}$. However, with the interactions of Ref. [14] we only consider $\mathbf{j}_{\pi \mathrm{IV}}^{(1)}$.

These currents have power law behavior at large momenta, and need to be regularized before their matrix elements between nuclear wave functions can be calculated (incidentally, we note that these calculations are done here in r-space). We adopt two different regularization schemes depending on whether the interactions used to generate the wave functions are in momentum space the 2N N4LO interactions of Refs. [14]—or in configuration space—the 2N N3LO interactions of Ref. [11]. In the former case, the momentum-space two-body currents are multiplied by a cutoff function of the form $C_{\Lambda}(p) = e^{-(p/\Lambda)^4}$ with p equal to the momentum transfer k_i to nucleon i in the seagull piece of Eq. (2.7) and in Eqs. (2.11), and (2.15)-(2.16), or equal to the relative momentum k in the pion-in-flight term of Eq. (2.7)and in Eqs. (2.12) and (2.18). As already noted, we do not retain the Δ -excitation current of Eq. (2.9) with the interactions of Ref. [14]. Fourier transforms are then reduced to one-dimensional integrations, which are easily carried out numerically.

When using the chiral interactions of Ref. [11], we first carry out the Fourier transforms of the various currents, resulting in configuration-space operators which are highly singular at vanishing inter-nucleon separations, and then remove this singular behavior by multiplying the various terms by appropriate r-space cutoff functions, identical to those used in Ref. [11] for the 2N interaction. The procedure as well as the explicit expressions for the resulting currents can be found in Ref. [15].

III. DETERMINATION OF LOW-ENERGY CONSTANTS

In this section we proceed to the determination of the LECs d'_8 , d'_9 , d'_{21} , C'_{15} and C'_{16} entering the current operators at N3LO. Before discussing fitting procedures, we introduce the various nuclear interaction models and provide references to the numerical methods used in the calculation of the various observables.

In this study we consider two different sets of interaction models. The first consists of the Norfolk models (denoted as NV) from Ref. [11]. These are N3LO chiral interactions that include, beyond pion and nucleon, Δ -isobar degrees of freedom explicitly. They are formulated in configuration space with two regulators, $R_{\rm S}$ and $R_{\rm L}$ respectively, for the short-range (contact) component and long-range (one- and two-pion exchange) component. There are two classes of NV interactions, which differ in the range of lab energy over which the fits to the 2Ndatabase were carried out. The first, denoted as NVI, was fitted in the range 0–125 MeV, while for the second, denoted as NVII, this range was extended to 200 MeV. Within each class, two different sets of cutoff values $R_{\rm S}$ and $R_{\rm L}$ were considered, and the resulting models were designated as NVIa/b or NVIIa/b (see Table I).

The second set of interaction models are those developed by Entem, Machleidt and Nosyk (EMN) in Ref. [14].

Name	DOF		$(R_{\rm S}, R_{\rm L})$ or Λ		Space
NVIa	π, N, Δ	N3LO	(0.8, 1.2) fm	$0-125~\mathrm{MeV}$	r
NVIb	π, N, Δ	N3LO	(0.7, 1.0) fm	$0125~\mathrm{MeV}$	r
NVIIa	π, N, Δ	N3LO	(0.8, 1.2) fm	$0-200~\mathrm{MeV}$	r
NVIIb	π, N, Δ	N3LO	(0.7, 1.0) fm	$0200~\mathrm{MeV}$	r
EMN450	π, N	N4LO	$450~\mathrm{MeV}$	$0-300~{\rm MeV}$	p
${\rm EMN500}$	π, N	N4LO	500 MeV	$0300~\mathrm{MeV}$	p
EMN550	π, N	N4LO	$550~\mathrm{MeV}$	$0300~\mathrm{MeV}$	p

TABLE I. Summary of 2N interaction models utilized in this study. In the first column we indicate the name adopted to identify each model and in the remaining columns its main features, including degrees of freedom (DOF), chiral order (O_χ) , cutoff values, lab-energy range over which the fits to the 2N database have been carried out (E range), and whether it is in configuration (r) or in momentum (p) space.

These are momentum-space chiral interactions including only pions and nucleons as degrees of freedom. The regularization is implemented in momentum space as well, and as a consequence these models, in contrast to the NV ones, are strongly non-local in configuration space. For this set of interactions, which have all been fitted to the 2N database up to 300 MeV lab energy, three different cutoff values, respectively $\Lambda=450$, 500 and 550 MeV, are considered. All chiral orders are available for these models and so, as discussed below, fits of the electromagnetic LECs were carried out order-by-order from NLO to N4LO. However, we will report only the values corresponding to the N4LO interactions, if not otherwise specified.³ All the interactions considered in the present study along with their main features are listed in Table I.

In the calculations of A=3 observables, we include (chiral) three-nucleon (3N) interactions at LO (in particular, for the NV models we also account for the LO two-pion-exchange term originating from Δ -resonance intermediate states [12]). The LECs (c_D and c_E , in standard notation) that characterize them have been constrained by reproducing the ³H-³He binding energies and the Gamow-Teller matrix element in tritium beta decay. We take the LECs from Table III of Ref. [16] for the NV set of 2N interactions and from Table II of Ref. [17] for the EMN set. In the following, we will denote with the * superscript the NV Hamiltonians consisting of these 2N and 3N interactions. The * is to differentiate them from the NV Hamiltonians in which the 3N interactions are fitted to reproduce a different set of trinucleon observables [12] (³H-³He binding energies and nd doublet scattering length). The A=3 wave functions have been obtained from solutions of the Schrödinger equation with the hyperspherical-harmonic approach [18, 19].

³ Values for the electromagnetic LECs obtained with the lower order EMN interactions are available from the authors upon request.

The calculation of the A=2-3 magnetic form factors and magnetic moments is performed using Monte Carlo integration techniques [20]. The number of sampled configurations utilized is of the order of 10^6 for the deuteron and 5×10^5 for the A=3 systems. The statistical errors due to these Monte Carlo integrations are typically $\lesssim 1\%$ over the range of momentum transfers considered. In the final results these errors are summed up in quadrature with uncertainties from other sources we account for in the present study (see below).

The cross section for the deuteron threshold electrodisintegration at backward angles (d-threshold) has been obtained by evaluating the relevant matrix elements of the electromagnetic current between the ground state and np continuum states using standard Gaussian quadrature methods [15, 27]. While the d-threshold experimental data have been averaged over the interval 0–3 MeV of the final np-pair center-of-mass energy, the theoretical results have been computed at a fixed energy of 1.5 MeV. It is known that the effect of the width of the energy bin over which the cross-section values are averaged is small [27].

We can now discuss the fit of the electromagnetic LECs entering the OPE and non-minimal contact currents at N3LO. We introduce the set d_i^S and d_i^V of adimensional LECs—the superscript specifies the isoscalar (S) or isovector (V) character of the associated operators—in units of m_{π} (cutoff Λ) for the NV (EMN) Hamiltonians, namely

$$C'_{15} = d_1^S/\lambda^4 , \quad d'_9 = d_2^S/\lambda^2$$

 $C'_{16} = d_1^V/\lambda^4 , \quad d'_8 = d_2^V/\lambda^2 , \quad d'_{21} = d_3^V/\lambda^2 ,$ (3.1)

with $\lambda=m_\pi$ or Λ for the NV or EMN Hamiltonians, respectively. Their corresponding values are reported in Tables II and III. We fitted the LECs using a χ^2 minimization procedure on two different sets of data. Set A includes the magnetic moments of deuteron (μ_d) , tritium $(\mu_{^3\mathrm{H}})$, helium $(\mu_{^3\mathrm{He}})$ [26] and the d-threshold cross sections data up to $q_\mu^2=40~\mathrm{fm^{-2}}$ [21–25], whereas set B includes the A data set plus the deuteron magnetic form factor $G_M(q_\mu)$ data up to momentum transfers of $q_\mu=6~\mathrm{fm^{-1}}$. The star superscript indicates that from the sets A and B we have removed the d-threshold cross-section data corresponding to the Rand et al. experiment of 1967 [21]. While these data do not impact significantly the determination of the LECs, they do produce a large increase in the χ^2/datum .

In the present study we carry out a simultaneous fit of these data sets, without separating them in (predominantly) isoscalar and isovector observables. Thus, we are able to account explicitly for the fact that the trinucleons are not pure isospin T=1/2 states, but also include small T=3/2 admixtures, induced by isospin symmetry-breaking interaction terms present in the NV and EMN Hamiltonians. Furthermore, in the d-threshold cross-section calculations, we include all continuum states and not just the dominant $^1\mathrm{S}_0$ channel. Note that the present

~	1V	1V	•V	.0	.0	2 /27
Set	d_1^V	d_2^V	d_3^V	d_1^S	d_2^S	χ^2/N
			$NVIa^*$			
Α	-0.050(2)	0.49(7)	0.094(4)	0.012(1)	0.023(7)	11.0
A^{\star}	-0.050(2)	0.59(6)	0.109(4)	0.012(1)	0.028(9)	2.6
В	-0.052(1)	0.45(3)	0.093(3)	0.011(1)	0.032(8)	12.4
B^{\star}	-0.050(1)	0.61(6)	0.114(6)	0.009(1)	0.044(6)	3.9
			$NVIb^*$			
Α	-0.055(3)	0.09(5)	0.073(3)	0.025(2)	0.030(6)	11.0
A^{\star}	-0.053(1)	0.18(3)	0.086(3)	0.029(2)	0.044(8)	2.7
В	-0.057(1)	0.07(3)	0.073(3)	0.026(2)	0.038(6)	12.0
B^{\star}	-0.052(2)	0.21(4)	0.090(4)	0.030(2)	0.052(5)	3.6
			NVIIa*			
Α	-0.066(2)	0.01(7)	0.069(4)	0.011(1)	0.019(7)	11.0
A^{\star}	-0.064(3)	0.15(9)	0.086(5)	0.011(1)	0.020(8)	2.6
В	-0.068(2)	-0.03(5)	0.069(3)	0.010(1)	0.025(8)	12.0
B^{\star}	-0.067(1)	0.10(5)	0.087(5)	0.009(1)	0.040(8)	3.5.
			NVIIb*			
Α	-0.049(2)	0.09(4)	0.048(3)	0.017(1)	0.018(3)	12.5
A^{\star}	-0.048(3)	0.17(5)	0.060(4)	0.019(2)	0.022(4)	3.2
В	-0.050(3)	0.08(4)	0.047(3)	0.017(1)	0.020(3)	13.4
В*	-0.050(3)	0.14(3)	0.058(3)	0.020(2)	0.027(5)	4.0.

TABLE II. Adimensional values of the LECs corresponding to the NV Hamiltonians Ia*, Ib*, IIa*, and IIb* fitted to various data sets; see text for more details.

strategy for constraining the LECs is different from that adopted in Refs. [8, 15], where resonance saturation arguments were invoked to reduce their number and only the magnetic moments of $A\!=\!2$ and 3 nuclei and/or the radiative capture cross section for thermal neutrons on protons were fitted.

The LECs of Tables II and III are generally in line with the expected values based on the naive power counting given in Ref. [15]. However, d_2^V is too large by a factor of 10–20 for all Hamiltonian models we have considered, as is d_2^S corresponding to the data sets A and A* for the EMN500 and EMN550 models. Lastly, the LEC d_1^V for the EMN500 and EMN550 interactions is poorly constrained by the fits, and so it is difficult to have a meaningful comparison with the naive power counting.

In an attempt to improve the description of the deuteron $G_M(q_\mu)$ data at higher momentum transfers (thus, "stretching" significantly the regime of applicability of the present χ EFT framework), we included these data in the fits of the LECs (set B). However, this has a completely negligible impact, as can be seen in Fig. 1 where we compare the results for $G_M(q_\mu)$ obtained using the LECs corresponding to sets A and B. We also note that including the deuteron $G_M(q_\mu)$ data in the fits does not alter the description of all remaining observables we consider in the present study.

By removing the d-threshold data of Ref [21] (sets A* and B* of LECs), the reduced χ^2 decreases very substantially, reaching a value of ≈ 3 for the NV interactions (the total number of data is of the order of 40 for set A and 65 for set B). It is worthwhile remarking here that we are fitting cross sections that fall by several orders of mag-

Set	d_1^V	d_2^V	d_3^V	d_1^S	d_2^S	χ^2/N					
-	EMN450										
Α	1.9(2)		0.39(2)	2.4(3)	0.08(10)	11.3					
A^{\star}	2.9(2)	6.7(1)	0.51(2)	2.0(3)	0.23(9)	2.8					
В	2.4(2)	6.4(1)	0.43(2)	3.32(6)	-0.29(3)	13.0					
B^{\star}	3.8(2)	7.2(1)	0.60(2)	3.36(6)	-0.31(3)	4.4					
			EMN5	000							
Α	-1.2(6)		0.55(3)		1.5(2)	14.7					
A^{\star}	-0.5(6)	4.6(3)	0.65(3)	2.2(2)	1.5(1)	4.7					
В	-0.2(6)	4.9(3)	0.57(3)	2.08(4)	0.33(7)	34.3					
B^{\star}	0.5(6)	5.2(3)	0.67(3)	2.09(4)	0.35(7)	24.5					
			EMN5	50							
Α	-0.6(1.5)	5.7(6)	0.31(5)	5.2(2)	6.2(4)	17.7					
A^{\star}	0.2(1.4)	6.0(6)	0.41(5)	5.3(2)	6.4(4)	7.9					
В	-0.3(1.5)	5.8(6)	0.26(5)	2.4(1)	-0.6(1)	34.1					
B^{\star}	0.8(1.5)	6.3(6)	0.36(5)	2.4(1)	-0.6(1)	24.9					

TABLE III. Same as for Table II, but for the EMN Hamiltonians corresponding to $\Lambda = 450,500$, and 550 MeV.

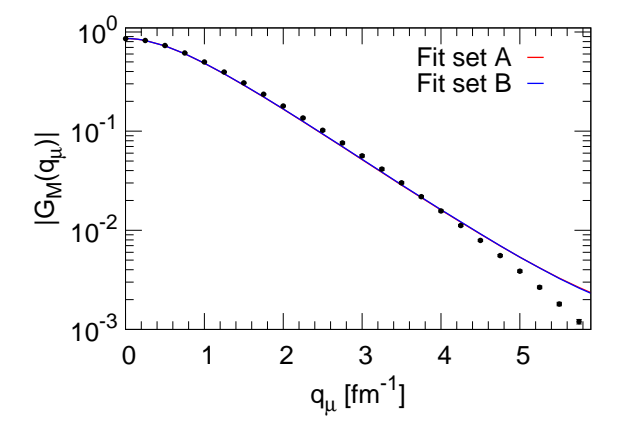


FIG. 1. Deuteron magnetic form factor computed using the NVIa interaction and corresponding to set A or B of LECs. The difference between the two curves cannot be appreciated. Similar results have been obtained with all the other interactions we consider. For clarity, errors have not been included in the figure.

nitude and span a region of momentum transfers q_{μ}^2 extending up to 40 fm⁻², in fact, well beyond the regime of validity of $\chi \rm EFT$. We also note that, overall, the quality of the fits for the other observables as well as the predictions for the A=2-3 nuclei magnetic form factors do not differ appreciably when using the un-starred and starred sets of LECs (the only exceptions are the EMN550-based predictions for the trinucleon magnetic form factors, see below). For this reason, hereafter we will discuss only the results obtained with set A of LECs.

Individual contributions, associated with the various terms of the current, to μ_d , $\mu_{^3\mathrm{H}}$, and $\mu_{^3\mathrm{He}}$, are reported in Tables IV, V and VI, respectively. The quoted errors are obtained by propagating the uncertainties on the fitted LECs. The Monte Carlo statistical errors are

also included (in quadrature) in the uncertainties quoted for the total results. The theoretical errors of these observables are less than one %. In general, the fit is able to reproduce a value compatible with experiment within the theoretical error bars, except for the EMN500 and EMN550 interactions in the deuteron magnetic moment case.

The μ_d observable receives contributions only from the isoscalar terms of the current. The results corresponding to the NV interactions obtained for the LO and N2LO are identical to those given in Ref. [15], but not for the N3LO(min) contribution or the contributions proportional to the refitted LECs d_1^S and d_2^S , for the reason explained above. Inspection of Table IV shows that (for the NV interactions) the N3LO OPE correction of Eq. (2.16) has opposite sign for models a and b, as in Ref. [15], where the origin of this sign flip is explained (see Fig. 3 of that paper). A sign flip also results between EMN450 or EMN500 and EMN550. Generally, the μ_d 's obtained with the EMN interactions tend to overestimate the experimental value. The main reason seems to be that the fits based on these models are not able to constrain the LEC d_2^S as for the NV cases.

Next, we discuss the results for the A=3 magnetic moments in Tables V and VI. We note that the row labeled N2LO includes only the contribution of the relativistic single-nucleon current ($\mathbf{j}_{\mathrm{RC}}^{(0)}$ in the notation of the previous section) for the EMN models. However, in the case of the NV models, this row also includes the contribution of the Δ -excitation current ($\mathbf{j}_{\Delta}^{(0)}$), which is dominant at N2LO and responsible for the sign flip. Both the NV and EMN interactions yield excellent fits of the experimental values of the trinucleon magnetic moments.

In Fig. 2 we present the results of the fit of the dthreshold data. The bands represent the error that has been calculated by propagating the uncertainties on the LECs with standard methods. All interactions reproduce nicely the data up to $q_{\mu}^2=30~{\rm fm^{-2}}$ (panels a and b for the NV models, and panel c for the EMN models). The q_{μ}^{2} behavior is sensitive to the interference between the fitted N3LO terms and the LO and (remaining) higher order terms in the current. For both the NV and EMN interactions the dominant interference is in the isovector sector for q_μ^2 in the range $10 \lesssim q_\mu^2 \lesssim 20 \ {\rm fm}^{-2}$. For $q_\mu^2 \gtrsim 20$ fm⁻², the interference in the isoscalar sector becomes significant and, in some instances, of the same magnitude as in the isovector sector. The EMN450 model stands out in that the interference in the isoscalar sector is dominant. For this model the fit appears to be unable to constrain the LEC d_2^S , generating the big error band that can be seen in panel c of Figure 2.

IV. MAGNETIC FORM FACTORS OF THE DEUTERON AND TRINUCLEONS

The d, ${}^{3}\mathrm{H}$ and ${}^{3}\mathrm{He}$ magnetic form factors corresponding to set A of LECs for all interaction models used

	NVIa*	NVIb*	NVIIa*	NVIIb*	EMN450	EMN500	EMN550
LO	0.8499	0.8486	0.8500	0.8501	0.8549	0.8564	0.8562
N2LO	-0.0062	-0.0062	-0.0065	-0.0071	-0.0069	-0.0070	-0.0074
N3LO(min)	0.0284	0.0301	0.0271	0.0242	0.0425	0.0317	0.0330
$N3LO(d_1^S)$	-0.0115(9)	-0.021(2)	-0.0100(9)	-0.014(1)	-0.029(4)	-0.012(2)	-0.0199(6)
$N3LO(d_2^S)$	-0.0015(4)	0.008(2)	-0.0011(4)	0.006(1)	-0.003(3)	-0.0049(8)	0.0094(6)
Total	0.859(6)	0.860(5)	0.860(6)	0.860(2)	0.859(10)	0.864(2)	0.871(2)
Exp.				0.8574			

TABLE IV. Individual contributions to the deuteron magnetic moment (in units of n.m.) corresponding to the NV and EMN 2N interactions. The errors on the d_i^S terms are only generated by the LECs (set A). The uncertainties quoted for the total are given by the sum in quadrature of the uncertainties due to the LECs and Monte Carlo integration.

	NVIa*	NVIb*	NVIIa*	NVIIb*	EMN450	EMN500	EMN550
LO	2.593	2.585	2.592	2.590	2.599	2.620	2.614
NLO	0.196	0.223	0.195	0.223	0.173	0.213	0.223
N2LO	0.032	0.057	0.031	0.054	-0.024	-0.026	-0.027
N3LO(TPE)	0.026	0.018	0.026	0.015	0.064	0.047	0.044
N3LO(min)	0.041	0.043	0.038	0.035	0.045	0.033	0.035
$N3LO(d_1^V)$	0.110(5)	0.106(5)	0.144(5)	0.090(4)	-0.046(4)	0.015(8)	0.01(1)
$N3LO(d_2^V)$	0.046(6)	0.130(7)	0.001(7)	0.139(7)	0.185(3)	0.090(7)	0.10(1)
$N3LO(d_3^V)$	-0.048(2)	-0.051(2)	-0.036(2)	-0.034(3)	0.024(1)	0.015(1)	0.006(1)
$N3LO(d_1^S)$	-0.014(1)	-0.026(2)	-0.013(1)	-0.017(1)	-0.037(5)	-0.015(2)	-0.024(1)
$N3LO(d_2^S)$	-0.003(1)	0.008(2)	-0.003(1)	0.006(1)	-0.004(5)	-0.015(2)	-0.005(0)
Total	2.98(1)	2.98(1)	2.98(1)	2.98(1)	2.98(2)	2.97(1)	2.97(2)
Exp.				2.979			

TABLE V. Same as Table IV for the tritium magnetic moment. Note the row labeled N2LO includes the contributions of both $\mathbf{j}_{\mathrm{RC}}^{(0)}$ and $\mathbf{j}_{\Delta}^{(0)}$ for the NV models, but only those of $\mathbf{j}_{\mathrm{RC}}^{(0)}$ for the EMN models.

in this study are compared with experimental data in Figs. 3, 4 and 5, respectively. In all figures the bands represent the uncertainties coming from the statistical errors in the Monte Carlo integration (albeit these errors are essentially negligible), and the propagation of the fitted LECs errors summed in quadrature. The error band expands because the relative weight of the N3LO terms and associated uncertainties becomes larger and larger as q_{μ} increases. These magnetic form factors represent predictions of our models. The trinucleon magnetic form factors have been normalized to unity at $q_{\mu}=0$.

The deuteron magnetic form factor obtained with the NV interactions is shown in Figs. 3a and 3b. Despite the more sophisticated fitting procedure adopted here than in previous works, we have very good agreement with experimental data only for $q_{\mu} \lesssim 3.5 \text{ fm}^{-1}$. At higher q_{μ} , theory overestimates the data; this overestimate is primarily due to the isoscalar spin-orbit term in the min current of Eq. (2.11) that is only partially corrected by the fitted (isoscalar) non-minimal term of Eq. (2.12). The isoscalar OPE contribution (at N3LO) is instead almost negligible.

The results for the EMN models in Fig. 3c show a similar, albeit more pronounced, behavior. In particular, for EMN500 and EMN550 the form factors are almost flat for $q_{\mu} \gtrsim 5 \text{ fm}^{-1}$. In these cases, the main contribution is again given by the contact (isoscalar) spin-orbit term

proportional to C_5 , which is especially large in the EMN models. Moreover, the q_{μ} falloff comes primarily from that of $G_E^S(q_{\mu}^2)$. The EMN500 also tends to underestimate the data in the region of $2 \lesssim q_{\mu} \lesssim 5 \text{ fm}^{-1}$.

The NV predictions for the trinucleon magnetic form factors with the present fitting procedure of LECs are generally in excellent agreement with the data up to $q_{\mu} \lesssim 4~{\rm fm^{-1}}$ as can be seen in Figs. 4a and 4b for $^3{\rm H}$ and Figs. 5a and 5b for $^3{\rm He}$ (with the exception of the NVIb* model). The fitted currents at N3LO are able to fill in the diffraction region generated at LO (by contrast, see Ref. [15]) and, particularly in the case of the NVIa*/IIa* models, reproduce well the minima seen in the $^3{\rm He}$ magnetic form factor. The interplay between the terms proportional to the LECs d_1^V and d_3^V and, in particular, the fine tuning between these LECs play a major role in achieving, at these high q_{μ} , such a level of success. Thus, the new procedure appears to validate the χEFT modeling of the electromagnetic current well beyond the $q_{\mu} \lesssim 2~{\rm fm^{-1}}$ limit of Ref. [15].

The picture for the EMN models is somewhat less satisfactory. The EMN450 model, as in the d case, completely fails to describe the data much beyond $q\gtrsim 3$ fm⁻¹. The EMN500 model provides the best description of the measured form factors, in fact at the same level of the NV interactions. The EMN550 reproduces poorly the data because of the large contribution proportional

	NVIa*	NVIb*	NVIIa*	NVIIb*	EMN450	EMN500	EMN550
LO	-1.775	-1.770	-1.774	-1.772	-1.767	-1.786	-1.783
NLO	-0.193	-0.221	-0.193	-0.220	-0.171	-0.211	-0.220
N2LO	-0.044	-0.070	-0.044	-0.068	0.009	0.011	0.011
N3LO(TPE)	-0.026	-0.017	-0.026	-0.014	-0.062	-0.045	-0.043
N3LO(min)	0.030	0.032	0.029	0.025	0.062	0.047	0.045
$N3LO(d_1^V)$	-0.107(4)	-0.104(5)	-0.141(5)	-0.088(4)	0.045(4)	-0.014(8)	-0.01(1)
$N3LO(d_2^V)$	-0.045(6)	-0.013(7)	-0.001(6)	-0.014(7)	-0.181(3)	-0.088(7)	-0.10(1)
$N3LO(d_3^V)$	0.047(2)	0.051(2)	0.035(2)	0.033(2)	-0.023(1)	-0.014(1)	-0.005(1)
$N3LO(d_1^S)$	-0.014(1)	-0.025(2)	-0.012(1)	-0.017(1)	-0.036(5)	-0.015(2)	-0.024(1)
$N3LO(d_2^S)$	-0.003(1)	0.008(2)	-0.002(1)	0.006(1)	-0.004(5)	-0.014(2)	-0.004(0)
Total	-2.13(1)	-2.13(1)	-2.13(1)	-2.13(1)	-2.13(2)	-2.13(1)	-2.13(2)
Exp.				-2.126			

TABLE VI. Same as Table V for the helium magnetic moment.

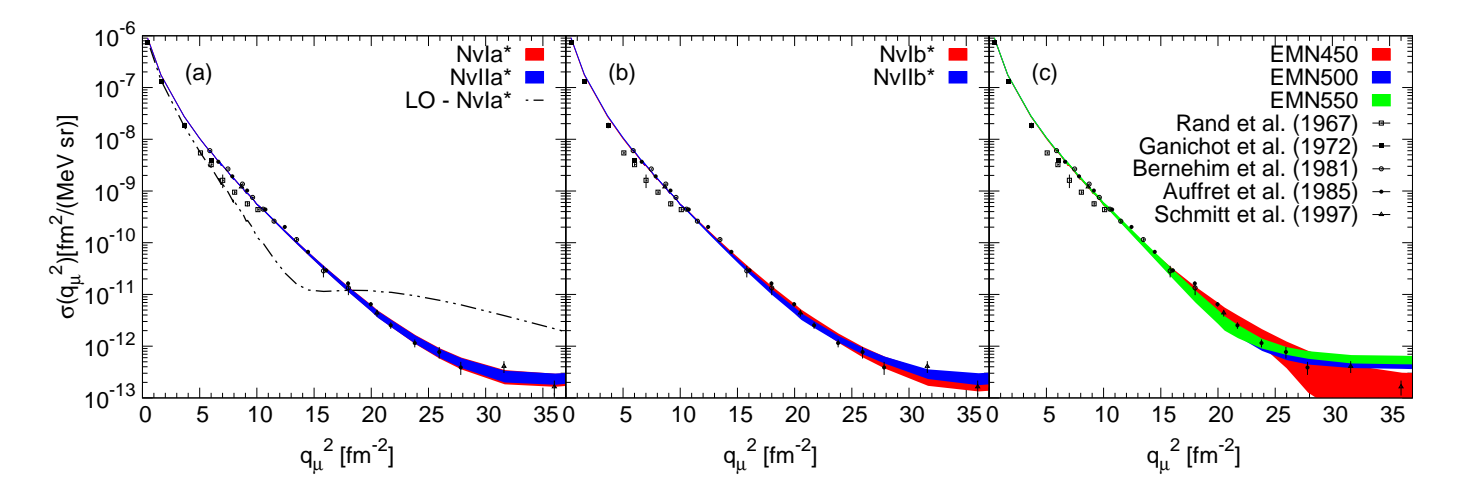


FIG. 2. The deuteron threshold electrodisintegration data at backward angles are compared to fits corresponding to interaction models NVIa* and NVIIa* in panel a, NVIb* and NVIIb* in panel b, and EMN450, EMN500, EMN550 in panel c. The bands represent the error that has been calculated propagating the uncertainties on the LECs with standard methods. The dashed line in panel a is the calculation performed with the LO current for the NVIa* interaction.

to d_2^S , which becomes dominant for $q_{\mu} \gtrsim 3 \text{ fm}^{-1}$. As a matter of fact, the d_2^S contribution resulting from the fit of the data set B (or B*) is much reduced, and provides a description of the trinucelon magnetic form factors similar to that obtained with the EMN500 model.

Because of the constraint on the LECs provided by the d-threshold cross-section data at high q_{μ}^2 , the present fitting procedure is much more successful in describing the magnetic form factors of the trinucleons at $q_{\mu} \gtrsim 2$ fm⁻¹ than reported previously in Refs. [8, 15]. The dominant isovector terms in the two-body currents convert spin/isospin S/T=0/1 pairs into S/T=1/0 pairs, and vice versa. Since in nuclei the correlated pair wave functions in these spin-isospin channels are similar in shape and only differ by a scale factor [28], one expects a similar scaling to occur in the two-body isovector transition densities, defined as

$$\rho^{2b}(r) = \langle \psi_{pn}(^{1}S_{0}) | \sum_{i < j} j_{ij,y}(q\hat{\mathbf{x}}) \, \delta(r_{ij} - r) | \psi_{d} \rangle \,, \quad (4.1)$$

in the deuteron, and as

$$\rho^{2b}(r) = \langle \psi_{3N} | \sum_{i < j} P_{ij}^{01} j_{ij,y}(q\hat{\mathbf{x}}) \, \delta(r_{ij} - r) P_{ij}^{10} | \psi_{3N} \rangle + \langle \psi_{3N} | \sum_{i < j} P_{ij}^{10} j_{ij,y}(q\hat{\mathbf{x}}) \, \delta(r_{ij} - r) P_{ij}^{01} | \psi_{3N} \rangle , (4.2)$$

in the trinucleons, where ψ_d and ψ_{3N} are, respectively, the deuteron and trinucleon wave functions, $\psi_{np}(^1S_0)$ is the np scattering wave function in the 1S_0 channel, $j_{ij,y}$ is the y component of the two-body isovector current (including all terms up to N3LO), and P_{ij}^{ST} is the projector operator over ST states for the pair ij. In Fig. 6 we show the densities corresponding to the NVIa* and EMN500 interactions. They have been computed at $q_{\mu} \approx 0.67$ and $3.45~{\rm fm}^{-1}$, and have been rescaled so as to peak at 1. As expected, the ratio of two-body current matrix elements in the d-threshold cross section and $^3{\rm H}/^3{\rm He}$ magnetic form factors is very nearly the same. Therefore, knowledge of these matrix elements in d-threshold is sufficient to predict the corresponding matrix elements in

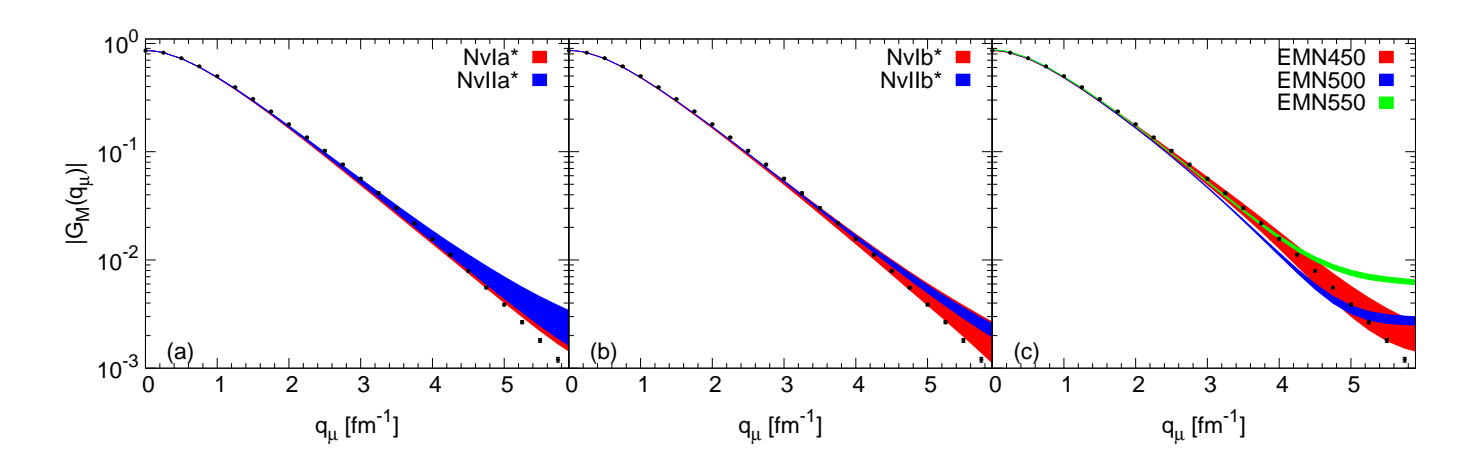


FIG. 3. The deuteron magnetic form factor is compared to predictions obtained with interaction models NVIa* and NVIIa* in panel a, NVIb* and NVIIb* in panel b, and EMN450, EMN500, EMN550 in panel c. The bands represent the error that has been calculated propagating the uncertainties on the LECs with standard methods. Note that in panel a the error bands almost coincide.

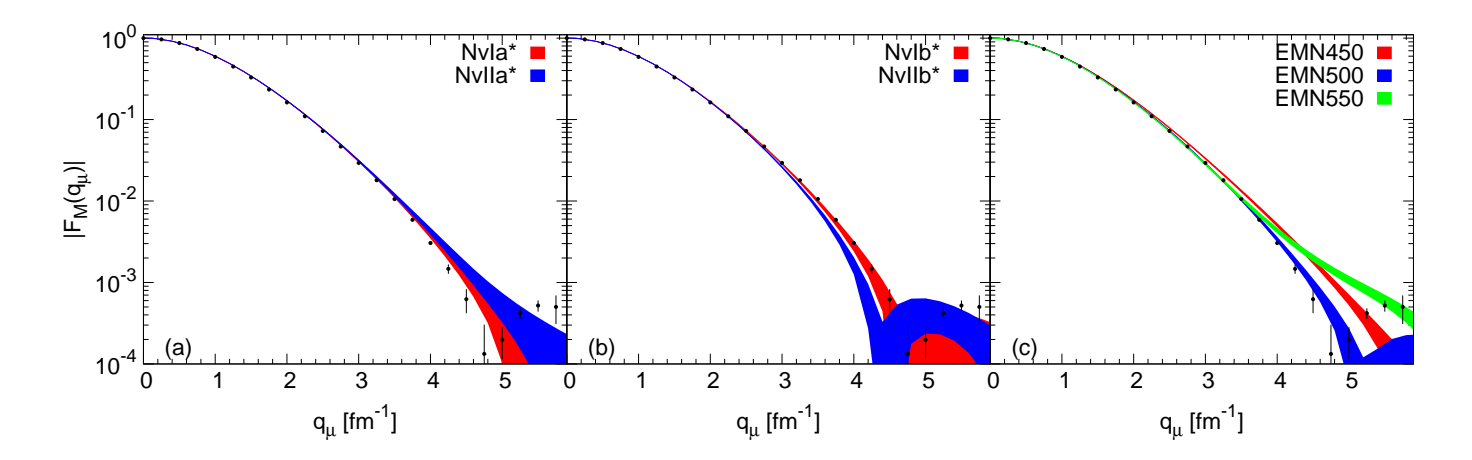


FIG. 4. The same as Figure 3 for the ³H magnetic form factor.

the ${}^3\mathrm{H}/{}^3\mathrm{He}$ form factors (or vice versa). In the region of $q_{\mu} \gtrsim 3.5~\mathrm{fm}^{-1}$, the contribution of two-body currents in these observables is dominant. It is then not surprising that, if we reproduce the d-threshold cross section in this q_{μ} -region, we will also be able to reproduce the trinucleon magnetic form factors. Incidentally, this scaling behavior also occurs in Gamow-Teller matrix elements of two-body weak currents in light nuclei [29].

We conclude this section by making a few remarks regarding the chiral convergence and the systematic errors generated by the truncation of the chiral expansion. As case study, we select the EMN500 model, which provides the best description of the trinucleon $F_M(q_\mu)$ and for which we have interactions at increasing orders, from LO to N4LO. While a Bayesian analysis based on Ref. [30] is ongoing, for the time being we carry out a study based on the approach by Epelbaum *et al.* [31]. For the observable $F_M(q_\mu)$, we consider two distinct expansions, one for

the nuclear interaction and one for the electromagnetic current. Therefore, we label the magnetic form factor as $F_M^{i,j}(q_\mu)$, where with i (NiLO, i=0 for LO) we indicate the order of the interaction and with j the order of the electromagnetic current at which $F_M(q_\mu)$ has been computed. To estimate the error due to the truncation of the interaction, we fix the current at N3LO, and then use the prescription of Ref. [31], namely

$$\Delta F_{M}^{I}(q_{\mu}) = \max \left[\alpha^{6} \times |F_{M}^{0,3}(q_{\mu})|, \right.$$

$$\alpha^{4} \times |F_{M}^{1,3}(q_{\mu}) - F_{M}^{0,3}(q_{\mu})|,$$

$$\alpha^{3} \times |F_{M}^{2,3}(q_{\mu}) - F_{M}^{1,3}(q_{\mu})|,$$

$$\alpha^{2} \times |F_{M}^{3,3}(q_{\mu}) - F_{M}^{2,3}(q_{\mu})|,$$

$$\alpha \times |F_{M}^{4,3}(q_{\mu}) - F_{M}^{3,3}(q_{\mu})| \right].$$

$$(4.3)$$

Similarly, for estimating the uncertainty due to the trun-

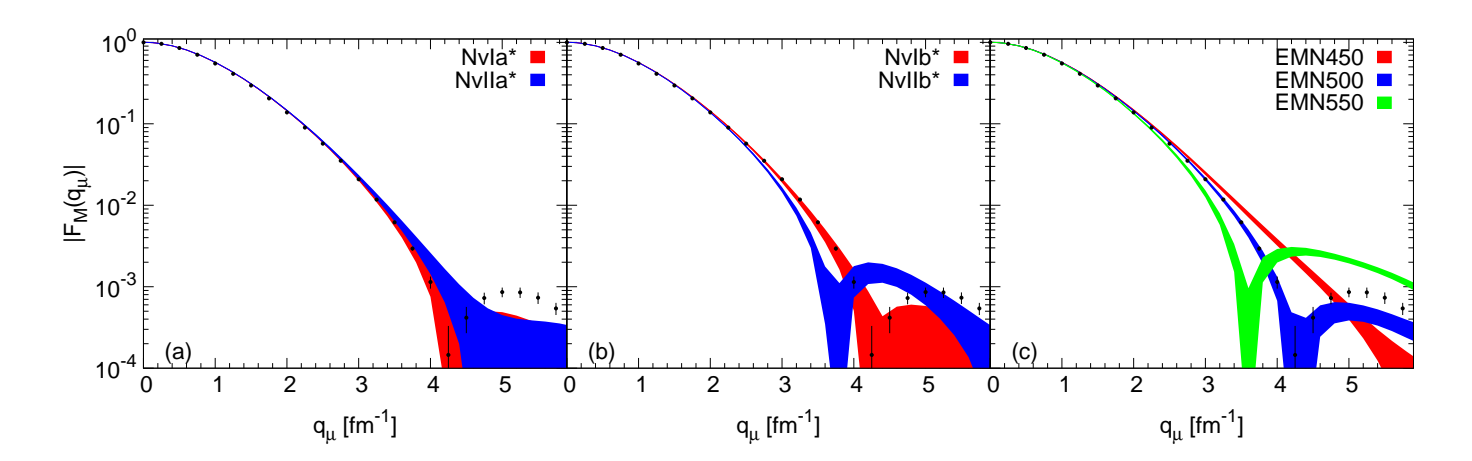


FIG. 5. The same as Figure 3 for the ³He magnetic form factor.

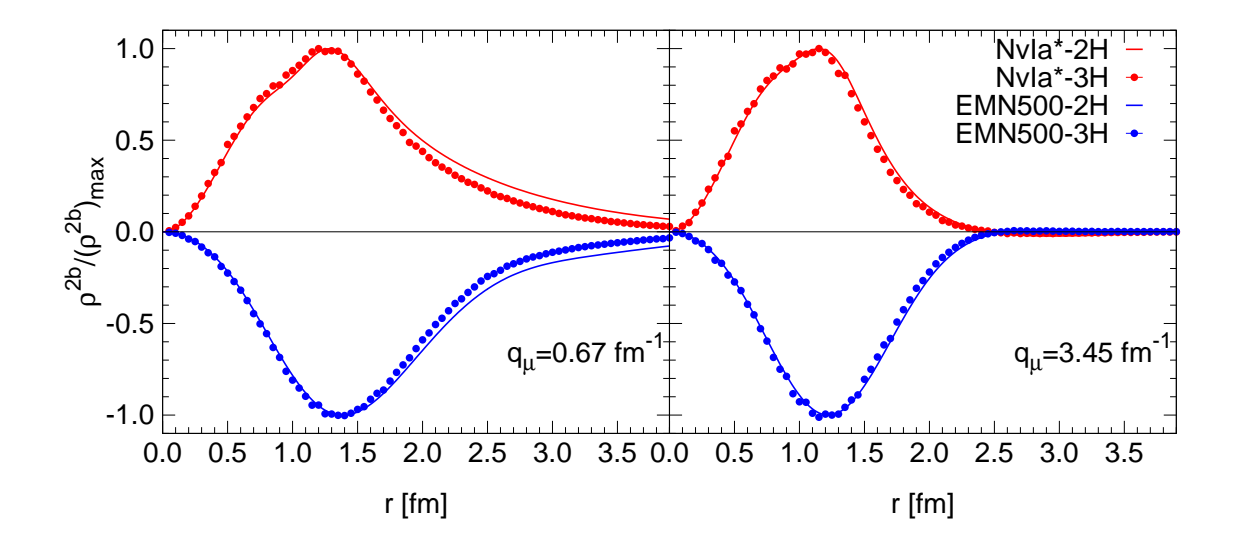


FIG. 6. Two-body transition densities corresponding to the NVIa* and EMN500 interaction models. All curves have been rescaled so as peak at 1. We inverted the sign of the EMN500 results to avoid clutter. The densities are computed at $q_{\mu} = 0.67$ fm⁻¹ (left panel) and $q_{\mu} = 3.45$ fm⁻¹ (right panel).

cation of the current, we fix the order of the interaction at N4LO, and evaluate

$$\Delta F_{M}^{C}(q_{\mu}) = \max \left[\alpha^{4} \times |F_{M}^{4,0}(q_{\mu})|, \right.$$

$$\alpha^{3} \times |F_{M}^{4,1}(q_{\mu}) - F_{M}^{4,0}(q_{\mu})|,$$

$$\alpha^{2} \times |F_{M}^{4,2}(q_{\mu}) - F_{M}^{4,1}(q_{\mu})|,$$

$$\alpha \times |F_{M}^{4,3}(q_{\mu}) - F_{M}^{4,2}(q_{\mu})| \right].$$

$$(4.4)$$

For simplicity, we assume that the two uncertainties are independent, and conservatively estimate the total uncertainty as

$$\Delta F_M(q_\mu) = \Delta F_M^I(q_\mu) + \Delta F_M^C(q_\mu).$$
 (4.5)

The expansion parameter α is taken as

$$\alpha = \max \left[\frac{|\mathbf{q}|}{\Lambda_{\chi}}, \frac{m_{\pi}}{\Lambda_{\chi}} \right], \tag{4.6}$$

where $|{\bf q}|$ is the magnitude of the three-momentum transfer and $\Lambda_\chi \simeq 1$ GeV. Of course, there is some degree of arbitrariness in the choice of α , since, for example, the external electromagnetic field, when it couples to a single nucleon, imparts a momentum ${\bf q}$ to this nucleon, while, when it couples to a pair of nucleons, will impart, on average, ${\bf q}/2$ to each nucleon in the pair.

In Fig. 7 we plot the results of the present analysis for the magnetic form factor of 3 He. The red boxes represent the systematic uncertainty $\Delta F_M(q_\mu)$. The red points are the central values and the bar represents the statistical

uncertainty due to the fitting procedure. It is immediately clear that this statistical uncertainty is almost negligible, when compared to the systematic one. The systematic uncertainty increases as q_{μ} increases, and seems to much reduce the predictive power of the theory for $q_{\mu} \gtrsim 3.8 \text{ fm}^{-1}$, albeit it should be noted that in that region the form factor has a zero.

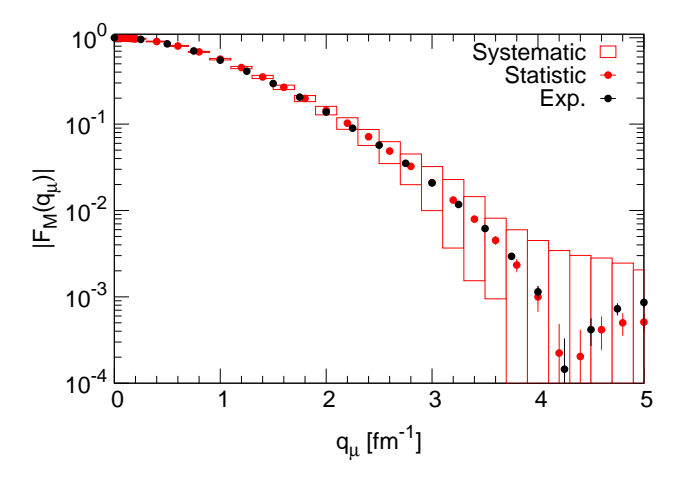


FIG. 7. The ³He magnetic form factor obtained with the EMN500 Hamiltonian model. The red boxes represent the uncertainties due to the truncation of the chiral expansion in the electromagnetic current and two-nucleon interaction (systematic). With the red bar we indicate instead the uncertainties produced by the fit of the LECs that appear in the electromagnetic current (statistical).

In Fig. 8 we show the result for the ³He magnetic form factor for selected values of q_{μ} order by order in the two-nucleon interaction, but with the current fixed at N3LO. The error bars on the red points represent only the systematic uncertainties $\Delta F_M^C(q_{\mu})$. For all the $q_{\mu} < 4$ fm⁻¹ considered the convergence of the chiral expansion appears to be satisfactory. At larger q_{μ} , the chiral expansion loses its predictive power and the systematic uncertainties dominate, as already observed in Fig. 7. It is also worthwhile noting that for $q_{\mu} = 1$ and 2 fm⁻¹, the point of convergence for the expansion appears to be off the experimental value. However, by adding the uncertainty due to the truncation of the chiral expansion in the electromagnetic current (blue points indicated by Final in Fig. 8), the theoretical predictions become compatible with the experimental values (within 2σ for $q_{\mu} = 1$ fm⁻¹).

Similar conclusions hold for the magnetic form factors of d and $^3{\rm H}$ obtained with the EMN500 interaction.

ACKNOWLEDGMENTS

We would like to thank Dr. Josh Martin for pointing out the mismatch in the labeling of the LECs entering the NLO contact terms of the NV interactions and the LECs of the minimal contact current. A.G. would like

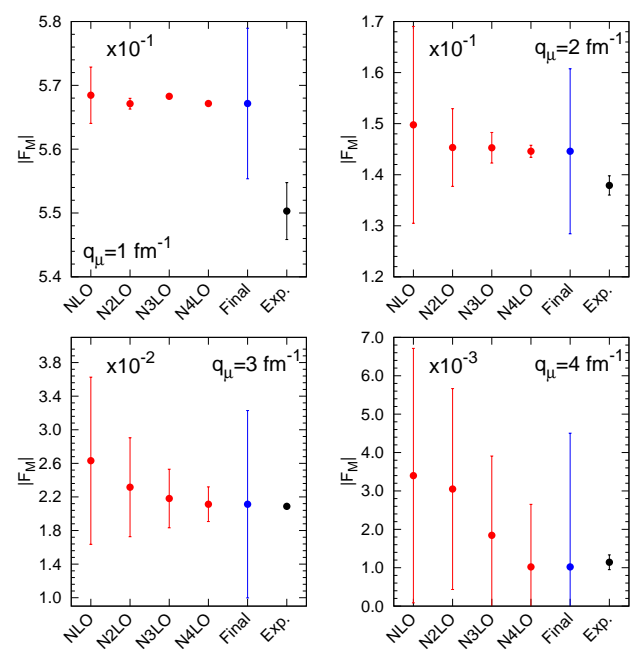


FIG. 8. Convergence results at selected values of q_{μ} for the ³He magnetic form factor. They are shown order by order in the expansion of the two-nucleon interaction, but with the electromagnetic current fixed at N3LO. The final points (blue) represent the full calculation, which includes in addition the systematic uncertainty due to the truncation of the electromagnetic current. The experimental values are also reported for comparison.

to thank all the LANL T2-group for the hospitality and the interesting discussions during his visit in Los Alamos. The support of the U.S. Department of Energy, Office of Science, Office of Nuclear Physics, under contracts DE-AC05-06OR23177. Computational resources provided by the National Energy Research Scientific Computing Center (NERSC) are also thankfully acknowledged.

S. Kölling, E. Epelbaum, and D.R. Phillips, Phys. Rev. C 86, 047001 (2012).

^[2] T.-S. Park, D.-P. Min, and M. Rho, Nucl. Phys. A596, 515 (1996).

^[3] S. Pastore, R. Schiavilla, and J. L. Goity, Phys. Rev. C 78, 064002 (2008).

^[4] S. Pastore, L. Girlanda, R. Schiavilla, M. Viviani, and R.B. Wiringa, Phys. Rev. C 80, 034004 (2009).

^[5] S. Kölling, E. Epelbaum, H. Krebs, and U.-G. Meissner, Phys. Rev. C 80, 045502 (2009).

^[6] S. Pastore, L. Girlanda, R. Schiavilla, and M. Viviani, Phys. Rev. C 84, 024001 (2011).

- [7] S. Kölling, E. Epelbaum, H. Krebs, and U.-G. Meissner, Phys. Rev. C 84, 054008 (2011).
- [8] M. Piarulli, L. Girlanda, L.E. Marcucci, S. Pastore, R. Schiavilla, and M. Viviani, Phys. Rev. C 87, 014006 (2013).
- [9] B. Kubis and U.-G. Meissner, Nucl. Phys. A 679, 698 (2001).
- [10] M. Piarulli, L. Girlanda, R. Schiavilla, R.N. Pérez, J.E. Amaro, and E.R. Arriola, Phys. Rev. C 91, 024003 (2015).
- [11] M. Piarulli, L. Girlanda, R. Schiavilla, A. Kievsky, A. Lovato, L.E. Marcucci, S.C. Pieper, M. Viviani, and R.B. Wiringa, Phys. Rev. C 94, 054007 (2016).
- [12] M. Piarulli, A. Baroni, L. Girlanda, A. Kievsky, A. Lovato, E. Lusk, L.E. Marcucci, S.C. Pieper, R. Schiavilla, M. Viviani, and R.B. Wiringa, Phys. Rev. Lett. 120, 052503 (2018).
- [13] C.E. Carlson, Phys. Rev. D 34, 2704 (1986).
- [14] D.R. Entem, R. Machleidt, and Y. Nosyk, Phys. Rev. C 96, 024004 (2017).
- [15] R. Schiavilla, A. Baroni, S. Pastore, M. Piarulli, L. Girlanda, A. Kievsky, A. Lovato, L.E. Marcucci, S.C. Pieper, M. Viviani, and R.B. Wiringa, Phys. Rev. C 99, 034005 (2019).
- [16] A. Baroni, R. Schiavilla, L.E. Marcucci, L. Girlanda, A. Kievsky, A. Lovato, S. Pastore, M. Piarulli, S.C. Pieper, M. Viviani, and R.B. Wiringa, Phys. Rev. C 98, 044003 (2018).
- [17] L.E. Marcucci, F. Sammarruca, M. Viviani, R. Machleidt, Phys. Rev. C 99, 034003 (2019).
- [18] A. Kievsky, S. Rosati, M. Viviani, L.E. Marcucci, and L. Girlanda, J. Phys. G 35, 063101 (2008).
- [19] L.E. Marcucci, J. Dohet-Eraly, L. Girlanda, A. Gnech, A. Kievsky, M. Viviani, Frontiers in Physics 8, 3389 (2020).

- [20] R. Schiavilla, V.R. Pandharipande, and D.O. Riska, Phys. Rev. C 40, 2294 (1989).
- [21] R.E. Rand, R.F. Frosch, C.E. Littig, and M.R. Yearian. Phys. Rev. Lett. 18, 469 (1967).
- [22] D. Ganichot, B. Grossetête, and D.B. Isabelle, Nucl. Phys. A178, 545 (1972).
- [23] M. Bernheim, E. Jans, J. Mougey, D. Royer, D. Tarnowski, S. Turck-Chieze, I. Sick, G.P. Capitani, E. De Sanctis, and S. Frullani, Phys. Rev. Lett. 46, 402 (1981).
- [24] S. Auffret, J.M. Cavedon, J.C. Clemens, B. Frois, D. Goutte, M. Huet, F.P. Juster, P. Leconte, J. Martino, Y. Mizuno, X.H. Phan, S. Platchkov, I. Sick, Phys. Rev. Lett. 55, 1362 (1985).
- [25] W.M. Schmitt, W. Turchinetz, C.F. Williamson, T.C. Yates, J.D. Zumbro, K.S. Lee, H. Baghaei, S. Churchwell, R.S. Hicks, R. Miskimen, G.A. Peterson, K. Wang, P.E. Bosted, M. Spengos, B. Frois, J. Martino, S. Platchkov, A. Hotta, Phys. Rev. C 56, 1687 (1997).
- [26] As reference values for the nuclear magnetic moments we used the NNDC catalog.
- [27] R. Schiavilla and D.O. Riska, Phys. Rev. C 43, 437 (1991).
- [28] J.L. Forest, V.R. Pandharipande, S.C. Pieper, R.B. Wiringa, R. Schiavilla, A. Arriaga, Phys. Rev. C 54, 646 (1996).
- [29] G.B. King, L. Andreoli, S. Pastore, M. Piarulli, R. Schiavilla, R.B. Wiringa, J. Carlson, S. Gandolfi, Phys. Rev. C 102, 025501 (2020).
- [30] J.A. Melendez, R.J. Furnstahl, D.R. Phillips, M.T. Pratola, S. Wesolowski, Phys. Rev. C 100, 044001 (2019).
- [31] E. Epelbaum, H. Krebs, and U.-G. Meissner, Eur. Phys.J. A 51, 53 (2015).